JARS Journal of Applied Remote Sensing

RESEARCH PAPER

Near real-time satellite detection and monitoring of aquatic algae and cyanobacteria: how a combination of chlorophyll-a indices and water-quality sampling was applied to north Texas reservoirs

Victoria G. Stengel,[a,*] **Jessica M. Trevino**,[b] **Tyler V. King**,[c] **Scott D. Ducar**,[c] **Stephen A. Hundt**,[c] **Konrad C. Hafen**,[c] **and Christopher J. Churchill**[d]

[a]U.S. Geological Survey Oklahoma-Texas Water Science Center, Austin, Texas, United States
[b]U.S. Geological Survey New York Water Science Center, Troy, New York, United States
[c]U.S. Geological Survey Idaho Water Science Center, Boise, Idaho, United States
[d]U.S. Geological Survey Upper Midwest Environmental Sciences Center, La Crosse, Wisconsin, United States

ABSTRACT. Aquatic algae and cyanobacteria can impair water-quality and pose risks to human and animal health. Several metrics of *in-situ* water-quality, including chlorophyll-a, phycocyanin, turbidity, Secchi depth, phytoplankton taxonomy, and hyperspectral reflectance, were collected in coordination with Sentinel-2 satellite overpasses to ascertain water-quality conditions and calibrate satellite detection and estimation of chlorophyll-a concentration. The performance of multiple satellite chlorophyll-a detection indices was evaluated by comparing satellite imagery to field observations of chlorophyll-a concentrations. Seventeen chlorophyll-a spectral indices were implemented using the ACOLITE atmosphere correction; the top performing indices were selected for further evaluation using the Sen2Cor and MAIN atmosphere corrections. The Moses three-band spectral index delivered the strongest linear agreement with field measurements of chlorophyll-a concentration across all reservoir sampling sites ($R^2 = 0.70$). Compared to open-water sites, the Moses three-band spectral index delivered better linear agreement with chlorophyll-a field measurements at inlet sites where there was a greater abundance of near surface aquatic chlorophyll-a concentrations, and the overall chlorophyll-a hyperspectral reflectance signal was stronger. Chlorophyll-a concentration estimates were implemented in a cloud-computation remote sensing platform designed for regional scale remote sensing analysis to map spatiotemporal patterns of aquatic chlorophyll-a across 10 study reservoirs located primarily in north Texas.

Published by SPIE [DOI: 10.1117/1.JRS.17.044514]

Keywords: remote sensing; chlorophyll-a; algae; cyanobacteria; Google Earth Engine; water resources; water-quality

Paper 230153G received Apr. 6, 2023; revised Aug. 17, 2023; accepted Oct. 2, 2023; published Nov. 15, 2023.

1 Introduction

Algae and cyanobacteria (commonly known as blue-green algae) are a speciose and functionally diverse group of photosynthetic microorganisms that are present in aquatic ecosystems worldwide.[1] The presence of certain types of algae and cyanobacteria potentially have nuisance or harmful effects on the water-quality in reservoirs. A reduction in dissolved-oxygen levels in aquatic ecosystems is associated with rapid increases in the population of algae and cyanobacteria

*Address all correspondence to Victoria G. Stengel, vstengel@usgs.gov

that can lead to anoxic fish kills and cause nuisance effects, including taste and odor producing biochemical compounds, such as geosmin and 2-methylisoborneol (MIB).[2–4] Toxins produced by certain cyanobacteria (i.e., cyanotoxins), such as microcystin, are known to cause skin irritation and acute and chronic toxicity.[5] Exposure to cyanotoxins can lead to illness or death in humans, pets, wildlife, and livestock through direct contact, inhalation, and ingestion or indirectly from the bioaccumulation of cyanotoxins in fish that are consumed as food.[6]

Algae and toxin-producing cyanobacteria are common in Texas reservoirs;[7] these reservoirs are extensively used for recreation and often serve as primary sources of drinking-water. This study emerged from existing regional water-quality monitoring efforts. A 2006 study by the U.S. Geological Survey (USGS) found that samples collected from 28 of 36 sampling sites representing 30 reservoirs in north Texas tested positive for at least one of three compounds (geosmin, MIB, or microcystin) produced by cyanobacteria.[7] In Texas, water-quality monitoring for cyanobacteria by the USGS began in 2016 in cooperation with Dallas-Fort Worth regional water resource authorities with the collection of baseline phytoplankton, chlorophyll-a, taste-and-odor compounds, and other toxin data from reservoirs used for drinking water.[8] Concerns regarding cyanobacteria increased when invasive aquatic Zebra mussels, *Dreissena polymorpha*, were detected in reservoirs in north Texas.[9] The presence of Zebra mussels can lead to the possible increase in concentrations of toxigenic species; however, the mutualistic relation between cyanobacteria and Zebra mussels is a topic of ongoing research.[10,11]

Cyanobacteria can release toxins at irregular times and under a myriad of conditions, making toxin concentrations difficult to predict.[9] Although the need for information on timing, extent, and constituency of algae and cyanobacteria is critical, monitoring for algae and cyanobacteria is challenging. A common approach is to rely on data obtained from periodically collected *in-situ* water samples to characterize large water bodies, and *in-situ* detections measured during an algae and cyanobacteria event. Consequently, the harmful or nuisance effects of algae and cyanobacteria often serve as the first notification that an event is occurring. Analysis of water-quality samples often requires a minimum of several days before laboratory results are available.[12] Thus, as the concern for harmful algae and cyanobacteria increases, timely identification is especially important for reservoirs that are used for recreation or drinking water supply.

Advancements in remote sensing technology, atmosphere correction (AC) science, and geocomputation capabilities are rapidly improving the ability to detect and deliver timely water-quality information to reservoir managers. Satellite sensors offer a range of spectral, spatial, and temporal resolutions that can be used to expand the perspective from local to regional scale water-quality monitoring, which can help to fill monitoring gaps and deliver timely information where and when *in-situ* data are relatively sparse, and ultimately aid decision makers in rapidly dispatching personnel to test water quality.[12–16]

The first Landsat satellite was launched in 1972, and for more than 50 years, the use of satellite observations have contributed to the detection and monitoring of photosynthetic phytoplankton (including chlorophyll-a in algae and cyanobacteria).[17,18] Operational water-quality monitoring methods that rely on ocean color satellite sensors for monitoring chlorophyll-a[19] and cyanobacteria[20] are well established, providing relatively coarse spatial resolution for larger inland bodies of water. For example, Coffer et al.[18] observed that the annual frequency of detectable cyanobacteria in 135 Texas reservoirs, resolvable by use of the ocean color sensor Sentinel-3 (300 m spatial resolution), increases toward the Gulf Coast; Grapevine Lake had a low (10%) and Lake Palestine had a relatively high (60%) annual cyanobacterial frequency.[18]

Satellite observations such as those made by the European Space Agency's (ESA) Copernicus Sentinel-2 satellites[21] (hereinafter referred to as "Sentinel-2") can detect light reflected from chlorophyll-a, a green pigment present in both algae and cyanobacteria, at 10 to 20 m spatial resolution.[22,23] Chlorophyll-a reflects relatively more green light and absorbs relatively more red and blue light during photosynthesis such that the visible water-color transitions from blue to green as the concentration of phytoplankton increases.[24] In addition to visible light, the spectral resolution of Sentinel-2 captures the red-near-infrared (NIR) light reflectance/scattering peak from chlorophyll-a photosynthesis (prior to NIR absorption from water) known as the "red edge."[25] Chlorophyll-a is commonly used as a proxy indicator of algal and cyanobacteria presence.[25] Spectral indices that are designed to detect and estimate chlorophyll-a concentrations cannot differentiate cyanobacteria from algae.[12,23] Indices capturing the red-NIR

region of the electromagnetic spectrum are a known target for delivering successful results; however, it is recommended to test the performance for a range of indices when calibrating a previously uncalibrated study area.[26] King et al.[27] compiled 17 aquatic chlorophyll-a spectral indices applicable to Sentinel-2 spectral resolution. Chlorophyll-a detection is limited by the transparency depth in a reservoir water column, which varies across the light spectra and is dependent on water clarity.[28] Constituent detection depth varies across aquatic systems; for example, it was estimated to be <1 m when chlorophyll-a concentrations reach 10 μg/L.[29]

AC is a crucial part of capturing imagery from water surfaces by satellite because water absorbs most of the light, and the reflectance signals from water surfaces are influenced by atmospheric effects.[30] The total at-sensor radiance signal captured by satellite-based instruments is corrected for atmospheric effects to isolate the sunlight reflected from water, and therefore the photosynthetic phytoplankton present on the water surface, entrained within the water column, or both. AC procedures have advanced in recent years, providing a range of AC options for retrieving light reflectance from water.[30–33] Aquatic reflectance (AR) imagery is designed to capture light that is reflected from the water surface or transmitted through the surface after being reflected from within the water column.[16,31,33,34] In contrast to AR products, bottom of atmosphere surface reflectance (SR) imagery is designed to capture the reflectance of sunlight across the range of land-cover classes present on the surface of our planet.[33]

Efficient operational satellite earth observation monitoring has recently become possible.[35–37] Sentinel-2 image collections are ingested into the high-performance cloud-based remote sensing platform within approximately 1 day of acquisition, enabling global-scale satellite monitoring[35,38] and ultimately contributing to a shift in the field of remote sensing into an earth observation monitoring paradigm.[36] The efficient geoprocessing of image collections enables time-series analysis[39] and visualization of historical image collections, providing new insights into dynamic histories pertaining to water-quality conditions of inland waters.[40–42]

The goal of a regional-scale satellite-based monitoring approach is to better inform reservoir managers about the near real-time presence of algae and cyanobacteria, helping them to effectively respond as needed; however, there are challenges associated with near real-time satellite-based monitoring. Clouds frequently block the view of the reservoir surface. High winds increase water-surface roughness, resulting in sun glint and light scattering that interfere with the accurate detection of light reflectance and thus with the assessment of water-quality constituents, such as algae and cyanobacteria.[25] The composition of turbid productive waters varies depending on the concentrations of aquatic system constituents (i.e., suspended sediment, algal, and cyanobacteria concentrations) and can limit the depth of the detection of chlorophyll-a from satellite images. High NIR reflectance from turbidity and glint can lead to over-correction from AC procedures and result in negative reflectance values.[25] High turbidity has influenced spectral indices to overestimate chlorophyll-a concentrations.[43]

To provide better information on the concentrations of algae and cyanobacteria in north Texas reservoirs, the USGS in cooperation with the North Texas Municipal Water District and City of Dallas evaluated a collection of 17 spectral indices selected from the literature[27] and three atmosphere-correction procedures.[32–34] The collection of spectral indices and atmosphere-correction procedures were tested to optimize the performance of satellite detection of aquatic chlorophyll-a for 10 reservoirs in north Texas (and a small part of southern Oklahoma) during 2020.

2 Methods

A regional-scale satellite monitoring approach is described herein that is designed for use in the Google Earth Engine cloud-based remote sensing platform, along with a discussion for implementation as part of near real-time monitoring. The goals of this study were to (1) collect *in-situ* water-quality, phytoplankton taxonomy, and hyperspectral reflectance data to examine and advance the knowledge of the spatiotemporal patterns of the presence of algae and cyanobacteria within the study reservoirs; (2) evaluate 17 spectral chlorophyll-a indices obtained from the literature across three ACs by comparing their performance to *in-situ* chlorophyll-a measurements; and (3) implement the highest ranked index-AC combination to estimate chlorophyll-a concentration in the cloud-based remote sensing platform for regional scale near real-time reservoir monitoring (Fig. 1).

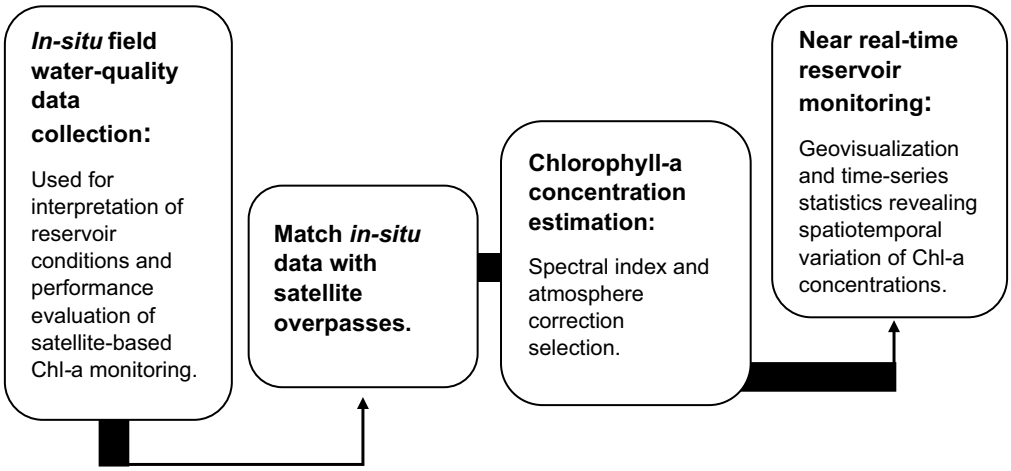

Fig. 1 Workflow diagram of the remote sensing geoprocessing for field water-quality data collection, matching, and interpretation to obtain chlorophyll-a (Chl-a) concentration estimates, and implementation in the cloud-based remote sensing platform for near real-time reservoir monitoring.

2.1 Study Area

The reservoirs sampled for this study include Lake Fork Reservoir, Grapevine Lake, Jim Chapman Lake, Lavon Lake, Lake Lewisville, Lake Palestine, Ray Hubbard Lake, Ray Roberts Lake, Lake Tawakoni, and Lake Texoma (Fig. 2). These reservoirs are within the Neches (Lake Palestine), Red (Lake Texoma), Sabine (Lake Fork Reservoir, and Lake Tawakoni),

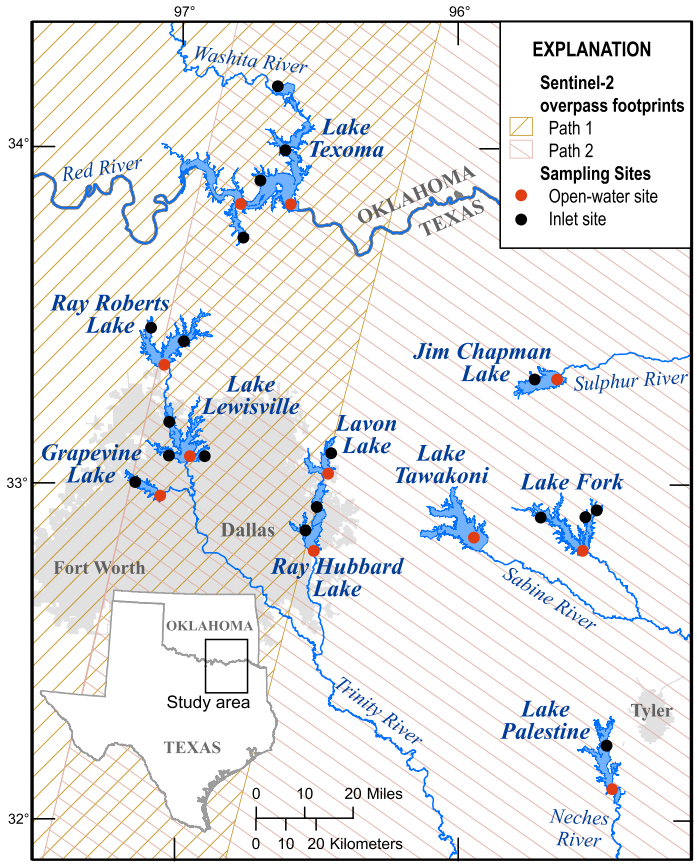

Fig. 2 Location of reservoirs, sampling sites, and Sentinel-2 overpass footprints within the study area in north Texas (including a small part of southern Oklahoma for three of the sites on Lake Texoma).

Sulphur (Lake Jim Chapman), and Trinity (Lakes Grapevine, Lavon, Lewisville, Ray Hubbard, and Ray Roberts) River Basins (Fig. 2). All reservoirs, except for Lake Texoma that forms the border between Texas and Oklahoma, are entirely in Texas.

These 10 reservoirs provide a collective capacity of more than 8.8 billion m^3 of developed water[44] and range in surface area from 27.9 to 317 km^2. Lake Fork Reservoir, Grapevine Lake, Lake Lewisville, Ray Hubbard Lake, Ray Roberts Lake, and Lake Tawakoni are used as sources of drinking water for the city of Dallas and surrounding areas. The City of Dallas has water rights for Lake Palestine, and this reservoir is expected to provide additional water resources to the Dallas area by 2027.[45]

2.2 Sampling Site Design

Thirty-one *in-situ* sampling sites were established across the 10 selected reservoirs (Fig. 2). At each reservoir, the sampling sites were divided into open-water (pelagic) sites and inlet sites. The Google Earth Engine LandTrendr Pixel Time Series Plotter was used to explore the spectral-reflectance histories of site locations, by plotting Landsat (1984 to 2022) time series of tasseled cap wetness and greenness spectral indices.[39] To account for the variability in spectral reflectance over the water surface of a given reservoir, different site selection criteria were used. At each reservoir, one or two open-water sites were selected near the center of the largest part of the water-surface area at deep locations where light reflection from the reservoir bottom would be considered negligible under normal reservoir capacity and where consistent tasseled-cap wetness and greenness time series spectral indices were obtained. In contrast to the open-water sites, inlet sites with interannual tasseled-cap wetness and greenness time series signals that varied were selected. As many as five inlet sites near tributaries, inlets, or coves per reservoir were selected. The sampling schedule and all of the water-quality data are provided in a companion USGS data release.[46]

2.3 Field Sampling

In-situ chlorophyll-a, phycocyanin, turbidity, water temperature, Secchi disk depth, phytoplankton taxonomy, and hyperspectral reflectance data were collected from boats during January to November 2020 to characterize a wide range of aquatic environments within each reservoir. The collection of *in-situ* chlorophyll-a samples was coordinated with Sentinel-2 overpasses. Wave action was avoided as much as possible for boat-operation safety and because surface roughness can increase light scattering, sun glint, and the occurrence of white caps, all of which can have negative effects on the spectra extracted from satellite imagery.[16] Thus, lower wind speeds are more suitable for both sampling and imagery analysis. Waterbody sampling was delayed when wind speeds were greater than 25 kph.

Water-quality field properties were measured using standard USGS sampling protocols.[47] The *in-situ* chlorophyll-a samples were grab samples collected at a depth of 0.3 m. The samples were chilled to 4°C and shipped on ice to the Trinity River Authority Central Laboratory in Dallas, Texas, for analysis. Chlorophyll-a concentrations were determined by using standard spectrophotometric methods,[48] and an ambient water reporting limit of 3 μg/L was set by the laboratory.[49] Reservoir water-clarity depth distributions across reservoir sampling sites were measured using a standard Secchi disk.[47] *In-situ* turbidity measurements were compared with the Secchi depth and chlorophyll-a concentration to aid in the interpretation of water-quality and water-clarity conditions on algorithm performance.[25] Phycocyanin, relative fluorescent units (RFU), turbidity, formazin nephelometric units (FNU), and temperature were measured *in-situ* with a YSI EXO2 multiparameter sonde.[50] A Kestrel 4500 pocket weather tracker was used to measure wind speed.[51]

Phytoplankton samples were collected and analyzed to identify dominant taxa across the reservoir open-water sampling sites and their spatiotemporal variability. The dominant algae and cyanobacteria taxonomy present at open-water sites in total biovolume (i.e., volume the individual algal organisms occupy in the water column), as well as the relative total biovolume (the percent total biovolume from the entire sample relative to all other taxa), were determined.[48,52–56] The phytoplankton samples were collected in 250-mL brown, opaque high-density polyethylene bottles and preserved on site with 2.5 mL of 0.25% glutaraldehyde solution. After collection, the phytoplankton samples were maintained at temperatures <4°C and shipped on ice to PhycoTech, Incorporated (PhycoTech in St. Joseph, Michigan) for analysis.

In-situ hyperspectral reflectance data were qualitatively compared with *in-situ* chlorophyll-a, phycocyanin, turbidity, and Secchi depth data to evaluate the hyperspectral reflectance observed for the Grapevine Lake sampling sites. Hyperspectral reflectance data were used to explore the optical signatures of algae and cyanobacteria pigments, chlorophyll-a, and phycocyanin, entrained in or accumulating on the water surface to aid in the interpretation of what portion of the spectrum might be most valuable for highly performing spectral indices.[57] Hyperspectral reflectance data of the water surface were obtained using an ASD HandHeld 2 visible NIR, 400 to 900 nm, spectroradiometer.[58] Boat shadows and sun glint were avoided during the collection of spectral reflectance signatures. The reflectance spectra were averaged during acquisition to minimize variations in brightness caused by movement of the water surface.

2.4 Satellite Sensors

The first Sentinel-2 satellite was launched in 2015 and was designed for monitoring global lands and waters.[21] The multispectral instrument (MSI) deployed on both the Sentinel-2a and Sentinel-2b satellites resulting in a combined revisit frequency of 5 days for the study area. The revisit frequency approximately doubles for reservoirs located where the 290 km overpass paths overlap (Fig. 2). The Sentinel-2 MSI sensor was selected because of its ability to detect the geophysical light reflectance of aquatic chlorophyll-a photosynthesis. Sentinel-2 offers expanded spectral resolution across the visible and NIR region of the electromagnetic spectrum compared with operational sensors; for example, the Landsat program was designed to monitor terrestrial vegetation that reflects brightly in NIR; however, the 800 nm (Landsat 8/9–band 5) frequency is absorbed by water. Sentinel-2 spectral resolution offers additional NIR bands capturing the "red edge" region of the spectrum. Sentinel-2 also provides advanced spatial resolution compared to operational inland (e.g., Landsat OLI) and ocean color sensors (e.g., Sentinel-3 OLCI). Sentinel-2 spatial resolution ranges from 10 to 60 m across the 13 spectral bands,[59] making it possible to obtain spectral data for narrow inlets with complex shoreline geometry. See Appendix Table 4 for central wavelength, bandwidth, and spatial resolution per spectral band.

2.5 Description of Atmosphere Corrections

Three AC procedures, ACOLITE,[32] MAIN,[32] and Sen2Cor[33] were combined with spectral indices to identify optimal index-AC equations. These ACs were selected for previously demonstrated performance and because they can be implemented in Google Earth Engine. The ACOLITE dark spectrum fitting AC approach[31,34] has been demonstrated to achieve global-leading performance for optical water types with elevated chlorophyll-a and suspended solids concentrations in a comparison of state-of-the-art aquatic ACs.[30] Imagery processed with ACOLITE was produced by downloading imagery from the ESA Copernicus portal and processing with ACOLITE locally for analysis. The Modified Atmospheric correction for INland waters (MAIN) calculates AR and is designed to run within the Google Earth Engine environment.[32] The Sentinel-2 Sen2Cor bottom-of-atmosphere reflectance image collection[33] is delivered by the ESA and is available in the Google Earth Engine data catalog as an analysis-ready dataset.[32]

2.6 Chlorophyll-a Detection Indices and Satellite Imagery Matches

The 17 chlorophyll-a detection spectral indices selected by King et al.[27] from the literature are applicable to Sentinel-2a/b based on the central wavelengths of spectral bands. Table 1 lists each index (also referred to as algorithms) that was tested herein and cites the paper that describes the equations represented by a given index name.[22,24,60–66] Semi-analytical ratio indices are simplified empirical approximations of radiative transfer theory, whereas derivative spectral shape indices quantify the curvatures of spectral shape.[25] Semi-analytical indices are sensitive, and derivative indices are designed to be less sensitive to the effects of atmosphere.[25]

The full *in-situ* chlorophyll-a dataset was initially matched with satellite imagery to maximize the sample size and to represent the range of conditions observed during this study. Filtering and masking logic were consistently applied across the three AC image collections to achieve a consistent comparison of index-AC performance.

A 90% cloud cover filter was applied to maximize the potential for matching *in-situ* water-quality data with satellite imagery across the regional study area. The Sentinel-2 operational

Table 1 Spectral indices tested for the study area.[27]

Index number	Index name	Index equation using Sentinel-2 spectral bands[a]	Citation
1	Be162Bsub	$b5 - b4$	Beck et al.[47]
2	BR23	$\frac{b2}{b3}$	O'Reilly et al.[24]
3	BR54	$\frac{b5}{b4}$	Gons et al.[60]
4	BR8a4	$\frac{b8a}{b4}$	Tebb et al.[61]
5	Go04MCI	$b5 - b6$	Beck et al.[62]
6	KIVU	$\frac{b2-b4}{b3}$	Beck et al.[59]
7	L83BDA	$\left(\frac{1}{b2} - \frac{1}{b4}\right) * b3$	Beck et al.[59]
8	FLHviolet	$b3 - (b4 + (b1 - b4))$	Beck et al.[59]
9	MCI	$b5 - b4 - (b6 - b4) * \left(\frac{704.1-664.6}{740.5-664.6}\right)$	Le et al.[63]
10	Moses3b	$\left(\frac{1}{b4} - \frac{1}{b5}\right) * b6$	Moses et al.[64]
11	NDCI54	$\left(\frac{5-b4}{b5+b4}\right)$	Mishra and Mishra[65]
12	NDCI8a4	$\left(\frac{b8a-b4}{b8a+b4}\right)$	Beck et al.[59]
13	S23BDA	$\left(\frac{1}{b4} - \frac{1}{b5}\right) * b8a$	Beck et al.[59]
14	FLHblue	$b3 - (b4 + (b2 - b4))$	Beck et al.[59]
15	SABI	$\left(\frac{b8a-b4}{b2+b3}\right)$	Beck et al.[59]
16	Toming	$b5 - \left(\frac{b4+b6}{2}\right)$	Toming et al.[22]
17	ZhFLH	$b8a - (b5 + (b4 - b5))$	Beck et al.[62]

[a]Detailed descriptions of Senintel-2 bands and their multispectral properties are available from the European Space Agency.[21]

cloud mask was applied for all image collections. Water detection and masking were applied using the normalized difference water index that utilizes Senintel-2 bands b3 and b8a (NDWI = (b3 - b8A)/(b3 + b8A)) to detect active water pixels and mask non-water pixels.[67] The chlorophyll-a spectral index value was retrieved using a 50 m radius for ACOLITE and 50 m diameter mean reducer for the MAIN and Sen2Cor image collections at each sampling site. *In-situ* chlorophyll-a samples were matched with satellite acquisitions nearest in time (± 2 days) to the sample date.

The satellite imagery matches were manually reviewed across all three image collections for consistency and image quality at the sampling sites. Matchups were eliminated from the analysis in cases of excessive sun glint and when cloud or water masking did not remove all clouds or cloud shadows in proximity to a sampling site. In addition, the image collection matchups were manually reviewed to verify that there were no negative values in the blue wavelength at the sampling sites as low AR values have the potential to be overcorrected by AC procedures.[25]

Because the ACOLITE AC is demonstrated to deliver high performance for waters with elevated concentrations of chlorophyll-a and suspended solids,[30] the chlorophyll-a detection indices were initially computed and ranked using ACOLITE in the R scripting environment.[68] If an index-ACOLITE combination achieved suitable performance metrics, then the index was tested across all three AC image collections.

2.7 Estimating Chlorophyll-a Concentration with Spectral Indices

Univariate linear regression models were developed to relate the value of each spectral index-atmospheric correction combination to the observed chlorophyll-a concentration, each with the following form:

$$\hat{Y} = \beta_0 + \beta_1 \times \text{Index}_i + \epsilon_i,$$

where $\hat{Y}$ is estimated chlorophyll-a concentration, β_0 is a fitted intercept, β_1 is a fitted coefficient, Index_i is the spectral indices considered, and ϵ_i is an error term. With this approach, modeled chlorophyll-a concentrations less than zero are possible, which is unrealistic. As a possible means of preventing negative chlorophyll-a concentrations, regression models in which chlorophyll-a concentration was log-transformed were tested;[24,69] however, increased heteroscedasticity in the residuals[70] of the log-transformed equations was observed when compared with equations using the untransformed chlorophyll-a observations. Thus, untransformed chlorophyll-a observations were used as the dependent variable in regression models. Negative chlorophyll-a estimates were retained for model evaluation. To ensure the use of linear regression models was appropriate, residual and Q-Q plots (not shown herein) were prepared and evaluated to qualitatively assess normality.[70]

The coefficient of determination (R^2)[70] resulting from a regression between observed chlorophyll-a and index-AC values was used to identify the top performing index-AC combination. Coefficients of determination were computed and ranked for the 17 spectral indices combined with ACOLITE. Spectral indices in which at least a moderate fraction of the variance was explained by the regression model ($R^2 > 0.5$) using ACOLITE were then computed and ranked for their performance with the Sen2Cor SR and the MAIN-based AR image collections. The relation between *in-situ* chlorophyll-*a* and *in-situ* turbidity was computed using the coefficient of determination. To explore and compare the spectral influence of turbid waters on the chlorophyll-*a* estimator across the three AC procedures, the coefficient of determination was computed from the top performing chlorophyll-*a* index and *in-situ* turbidity.

The linear regression models with the highest R^2 values for selected spectral indices that were used for chlorophyll-a concentration estimation were plotted with their corresponding prediction intervals and confidence intervals. The linear regression models were evaluated for performance across all sites, open-water sites, and inlet sites by comparing accuracy, precision, and bias.[69] Accuracy of predicted chlorophyll-a concentration values was assessed with both mean absolute error (MAE) and bias (systematic error), and root mean square error (RMSE) served as a measure of precision.[70] Although the RMSE and MAE metrics are similar, RMSE is influenced by outliers, whereas MAE is less sensitive to outliers.[69] Precision refers to the variability of the measurement error; the coefficient of variation (CV) was used to assess precision and is defined as the ratio of the standard deviation to the mean, thus expressing the extent of variability relative to the mean. Bias was measured as the average of the residuals, indicating under- or overestimation of the true value.[69]

The highest performing index-AC combinations were implemented in Google Earth Engine to produce reservoir-surface raster visualizations representing the spatial distribution of chlorophyll-a for visual comparison. Finally, a time series plot depicting the annual seasonal variation of chlorophyll-a was estimated for 50 m diameter mean values for all open-water and inlet sampling sites and filtered for cloud and sun-glint free satellite overpasses.

3 Results

3.1 Water-Quality and Reservoir Conditions

The chlorophyll-a concentrations measured in periodically collected *in-situ* water samples ranged from less than the reporting level of <3 to 87 μg/L; the turbidity ranged from 0.9 to 43.5 FNU, and the Secchi depth ranged from 0.06 to 2.83 m (Table 2). The phycocyanin fluorescence ranged from 0.18 to 5.25 RFU. The reservoir water temperature ranged from 10.1°C to 32.4°C.

The suitable satellite image overpasses ($n = 49$) were matched with 44 field chlorophyll-a samples acquired at open-water and inlet sites. No satellite imagery matches were achieved for Lake Fork because the synchronized image acquisitions did not meet image quality thresholds at this reservoir. The resulting data are presented in tabular and graphical form. Summary statistics including the range, mean, and median values for chlorophyll-a, turbidity, and Secchi depth are provided (Table 2). A scatterplot (Fig. 3) depicts the seasonal variation of *in-situ* chlorophyll-a with corresponding satellite imagery matches. For the nine reservoirs with satellite imagery matches, a sunburst diagram (Fig. 4) depicts *in-situ* chlorophyll-a concentrations that were matched with satellite imagery by sampling date and site for each of the reservoirs.

Table 2 Descriptive statistics of *in-situ* chlorophyll-a (chl-a), turbidity, and Secchi depth collected for this study and compared to the satellite imagery matches subset.

Data set	Site description	Statistic	Chl-a (μg/L)	Turbidity (FNU)	Secchi depth (m)
Satellite imagery matches	All sites	Range	<3 to 87	1.47 to 35.23	0.12 to 1.34
		Mean	29	8.71	0.65
		Median	25	6.23	0.55
	Inlet sites	Mean	36	11.88	0.49
		Median	37	8.93	0.43
	Open-water sites	Mean	22.26	5.14	0.72
		Median	21	4.25	0.67
All field data	All sites	Range	<3 to 87	0.9 to 43.5	0.06 to 2.83
		Mean	28.88	9.05	0.65
		Median	25	6.23	0.55
	Inlet sites	Mean	33.65	12.59	0.47
		Median	33.5	8.59	0.41
	Open-water sites	Mean	22.6	4.42	0.88
		Median	23	3.74	0.76

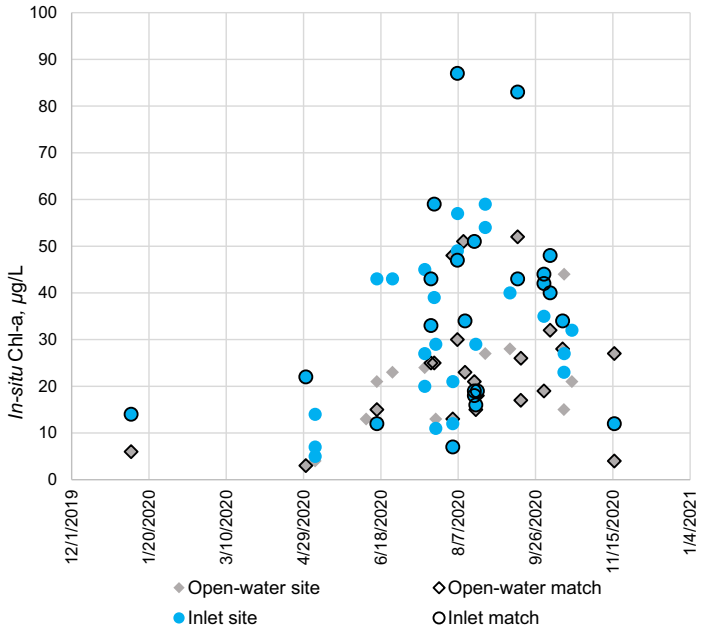

Fig. 3 Scatterplot depicting seasonal variation of *in-situ* chlorophyll-a (Chl-a) concentration collected in the field with the subset of corresponding satellite imagery matches for open-water and inlet sites, January to November 2020.

During the study period, all reservoirs were at some point dominated in relative biovolume by cyanobacteria (i.e., Cyanophyta); by contrast, Cryptomonads algae (i.e., Cryptophyta) and diatoms (i.e., Bacillariophyta) emerged as the dominant taxonomy less frequently for a subset of reservoirs.[46] Cyanobacteria from mid-June to mid-October dominated at most reservoirs except for the Jim Chapman Reservoir in August. Cyanobacteria had a larger dominance relative to other groups in the summer months (June to August) that declined in September and October. Bookending the cyanobacteria-dominated months were diatoms. Diatoms had the highest

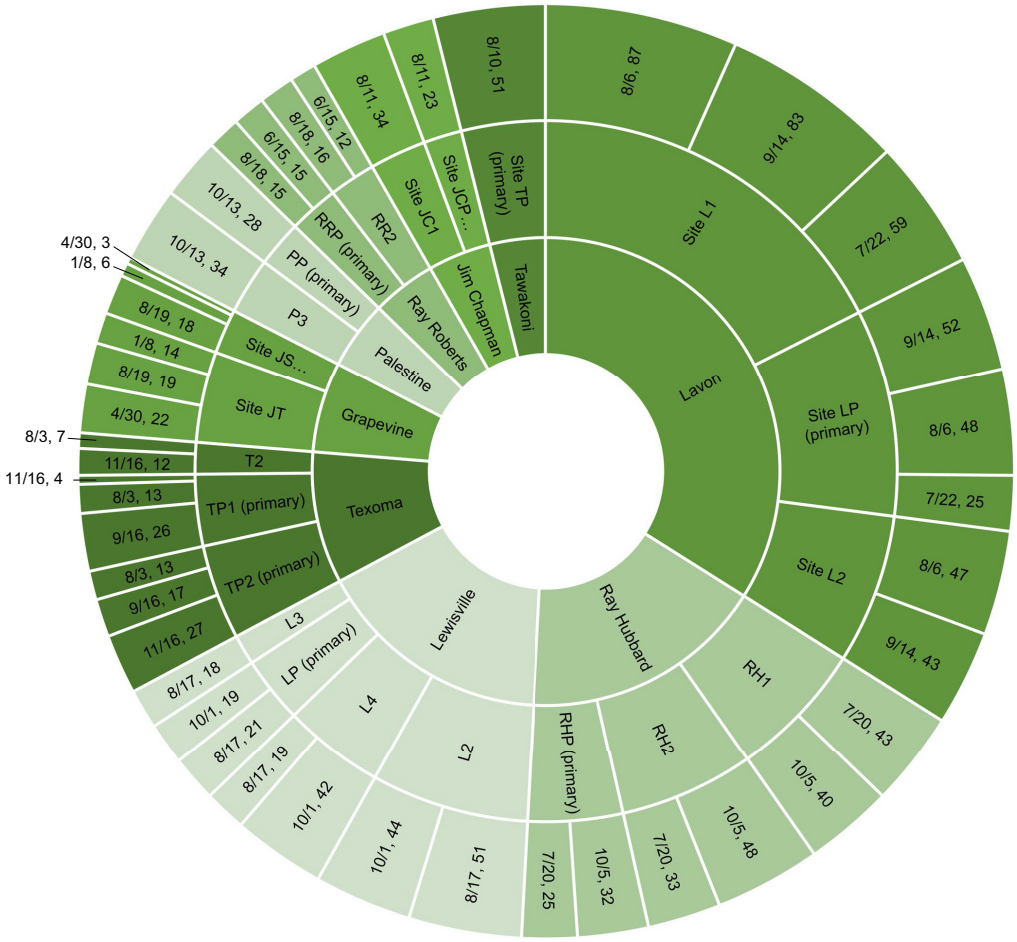

Fig. 4 *In-situ* chlorophyll-a concentrations in micrograms per liter (μg/L) with the sample date (outer ring), sampling site (middle ring), and reservoir (inner ring) matched with satellite imagery selected within ±2 days of a satellite overpass, January to November 2020. The width of the star-burst plot is representative of the observed *in-situ* chlorophyll-a concentration sample value. The various shades of green differentiate individual reservoirs.

relative biovolume from January to early June and then again in late October to November. The shift in dominance may be from relatively high water temperatures in north Texas during the late spring to early autumn. Butterwick et al. observed that the diatom, *Asterionella formosa*, had slightly lower growth rates than the cyanophyte, *Tychonem bourrellyi*, at temperatures above 25°C, whereas the reverse is true for temperatures below 10°C. Cryptomonads were dominant at only one point in time (April) at only one reservoir (Grapevine). Figure 5 depicts dominant phytoplankton taxonomy and sampling calendar dates. The companion data release[46] provides water-quality, phytoplankton taxonomy, and hyperspectral data for the sampling locations. Water-quality and phytoplankton taxonomy data are also stored in the USGS National Water Information System database (NWIS).[71]

3.2 Satellite Chlorophyll-a Detection Performance

The Moses three-band spectral index (Moses3b) produced the highest ranked R^2 values across all index-AC combinations led by the Sen2Cor AC. The results for all index-AC combinations are provided in the Appendix [Fig. 11]. Moses3b applied to ACOLITE, MAIN, and Sen2Cor yielded R^2 values of 0.66, 0.62, and 0.70, respectively, for all sites (Table 3). The Moses3b-Sen2Cor combination was selected and implemented as the chlorophyll-a estimator and further evaluated for performance (Fig. 6). All Moses3b AC combinations at inlet sites outperformed open-water sites in terms of the R^2 metric. The Moses3b-Sen2Cor combination delivered the lowest overall measure of MAE and RMSE for all sites, as well as for the inlet sites (Table 3). All three

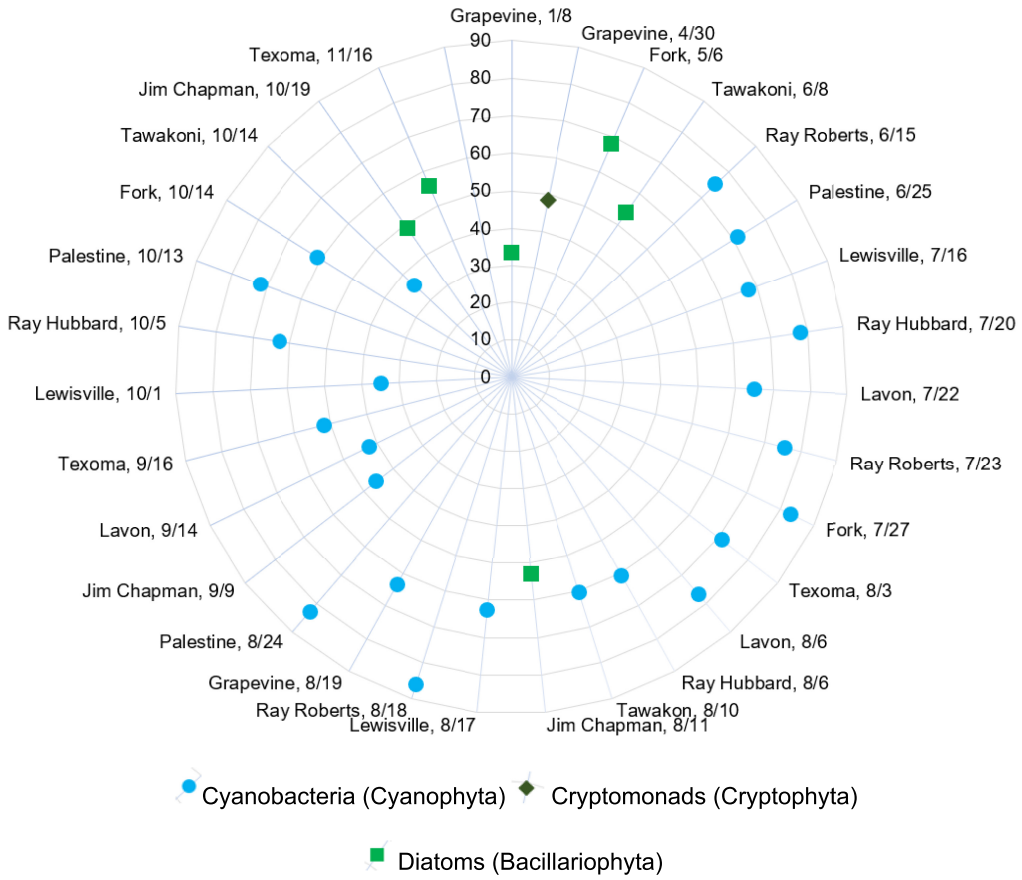

Fig. 5 Dominant phytoplankton taxonomy relative total biovolume (%) across reservoirs at open-water sampling sites, designated with sampling date, January to November 2020. Cyanobacteria are symbolized by a blue circle; cryptomonads are symbolized by a dark green diamond; and diatoms are symbolized by a green square.

Table 3 Aggregated performance metrics for the Moses3b chlorophyll-a detection spectral index comparing ACOLITE, MAIN, and Sen2Cor performance for sampling sites.

Statistic	ACOLITE	MAIN	Sen2Cor	Sample size	Site type
R^2 (μg/L)	0.66	0.62	0.70	49	All sites
	0.51	0.41	0.49	23	Open-water sites
	0.69	0.67	0.84	26	Inlet sites
RMSE (μg/L)	11	11.53	10.31	49	All sites
	10.21	11.03	11.44	23	Open-water sites
	11.66	12	9.2	26	Inlet sites
MAE (μg/L)	8.31	8	7.4	49	All sites
	8.18	8.36	8.45	23	Open-water sites
	8.43	7.69	6.48	26	Inlet sites
CV	54	51	52	49	All sites
	57	56	60	23	Open-water sites
	44	40	48	26	Inlet sites
BIAS (μg/L)	0	0	0	49	All sites
	1.33	0.19	3.13	23	Open-water sites
	−1.17	−0.16	−2.27	26	Inlet sites

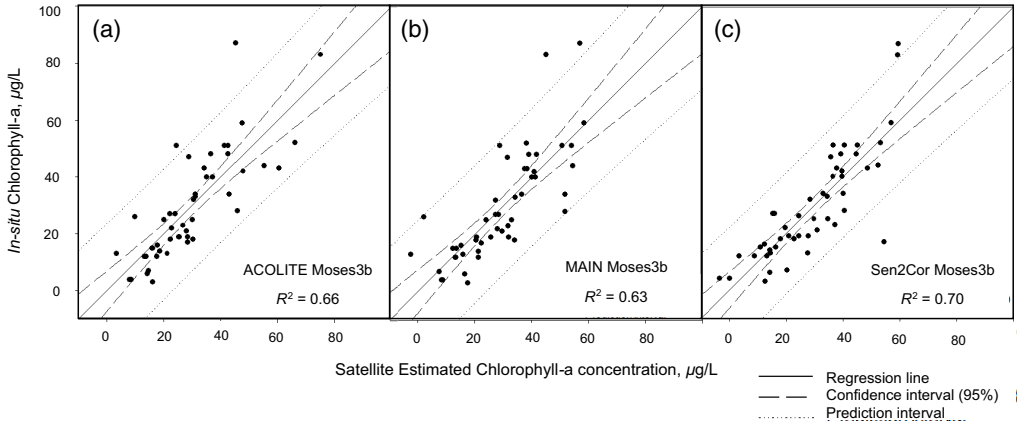

Fig. 6 Comparison of *in-situ* and satellite estimated chlorophyll-a concentration (μg/L) using the Moses3b index across all matchups applied to (a) ACOLITE AR, (b) MAIN AR, and (c) Sen2Cor SR.

Moses3b-ACs combinations produced similar variance magnitudes for all sites and the open-water and inlet classes. For the all sites group, the three combinations produced bias-free results (each delivered the same bias of 0 for all sites) and produced consistent positive bias for open-water sites and negative bias for inlet sites; refer to Table 3 for Moses3b performance comparison across ACs and site descriptions (all sites, inlet sites, and open-water sites). The correlation of *in-situ* chlorophyll-a and *in-situ* turbidity resulted in a low R^2 value ($R^2 = 0.35$) (Appendix Fig. 12). The influence of turbidity on the remotely sensed chlorophyll-a signal was evaluated by correlating the results of Moses3b values with *in-situ* turbidity. R^2 values ($R^2 = 0.11$ for ACOLITE, $R^2 = 0.33$ for MAIN, and $R^2 = 0.17$ for Sen2Cor) indicated that the influence of turbidity on the Moses3b index was consistently low (Appendix Fig. 13).

Grapevine Lake was used as an example for a qualitative comparison of index-AC combinations, *in-situ* water-quality data, and hyperspectral reflectance data because the August 19, 2020, site visit to this lake corresponded with high-quality satellite-imagery acquisition. The highest performing index-AC combination, Moses3b-Sen2Cor, was compared across the AC image collections and the highest-ranking indices to map and visualize aquatic chlorophyll-a concentrations (Figs. 7 and 8). In Fig. 7, chlorophyll-a concentration estimates obtained from the Moses3b index across the three ACs are compared {Sen2Cor [Fig. 7(a)], ACOLITE [Fig. 7(b)], and MAIN [Fig. 7(c)]}. In Fig. 8, the patterns of chlorophyll-a concentration estimates for the three highest performing chlorophyll-a indices applied to the Sen2Cor AC image collection are compared (Moses3b ($R^2 = 0.70$), S23BDA ($R^2 = 0.65$), and BR54 ($R^2 = 0.61$)] (Appendix Fig. 11).

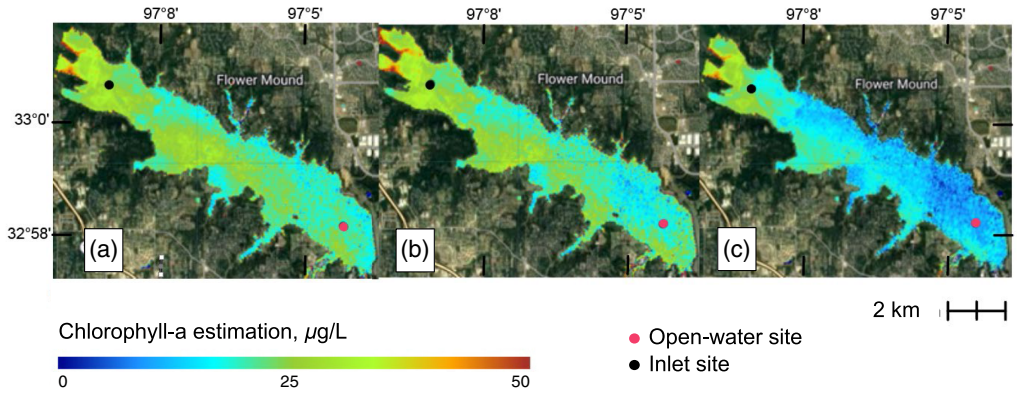

Fig. 7 Images of chlorophyll-a concentration estimates obtained from the Moses3b index obtained by applying the (a) Sen2Cor, (b) ACOLITE, and (c) MAIN ACs for Grapevine Lake, August 19, 2020.

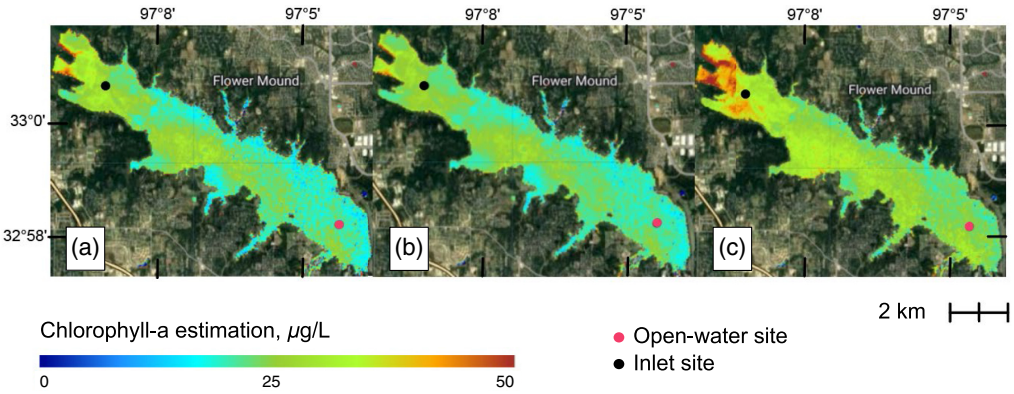

Fig. 8 Visual patterns of chlorophyll-a concentration estimates for the three highest-performing chlorophyll-a indices applied to the Sen2Cor AC image collection: (a) Moses3b, (b) S23BDA, and (c) BR54 for Grapevine Lake, north Texas, August 19, 2020.

Figure 9 depicts the relation between chlorophyll-a and phycocyanin spectral features acquired for the open-water and inlet sites compared with the Sentinel-2 spectral bands used in the chlorophyll-a detection indices (Table 1). The reflectance and absorption brightness magnitude of the spectrum indicate photosynthetically active waters with the unique spectral signature of cyanobacteria:[57] the green peak at about 560 nm (partially captured by Sentinel-2 band 3), the phycocyanin absorption trough at about 620 nm, the chlorophyll-a absorption trough at about 675 nm (partially captured by Sentinel-2 band 4), the NIR reflectance/scattering peak at about 700 nm (partially captured Sentinel-2 band 5), and NIR absorption by water at about 740 nm (partially captured Sentinel-2 band 6). Figure 9 shows there are more pronounced spectral features at the inlet site compared with the open-water site. The taxonomy observed at the open-water site was dominated by cyanobacteria.[46] *In-situ* chlorophyll-a concentrations, phycocyanin, and turbidity were concurrently higher at the inlet site than at the open-water site (chlorophyll-a

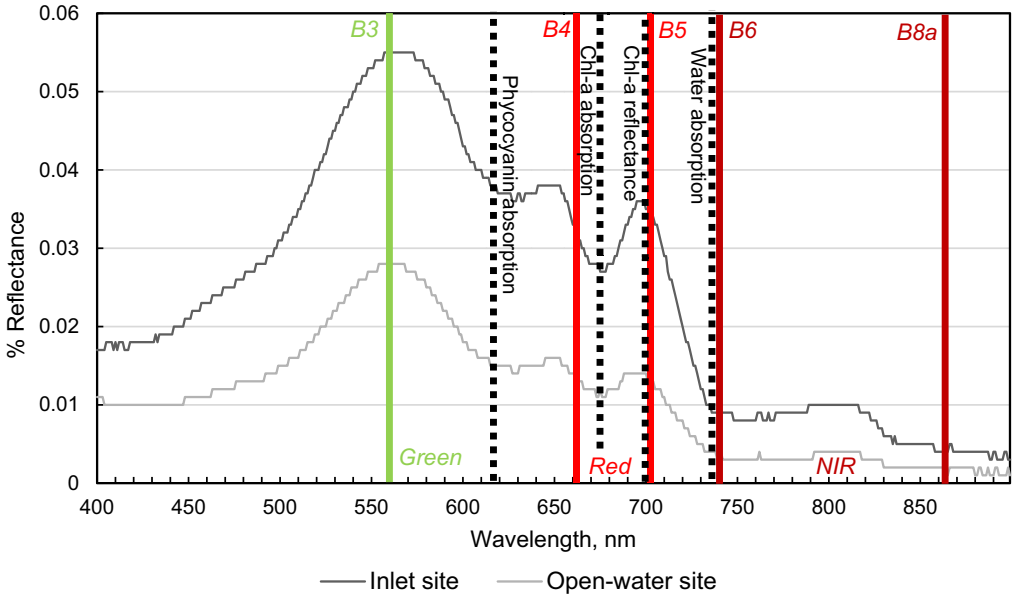

Fig. 9 *In-situ* hyperspectral reflectance from Grapevine Lake with selected Sentinel-2 spectral bands showing the magnitude and shape of chlorophyll-a and phycocyanin spectral features acquired August 19, 2020, for the inlet and open-water sampling sites. Solid vertical lines indicate light measured by Sentinel-2 spectral bands for green (band 3), red (band 4), red edge (band 5), and NIR (band 6 and band 8a); dashed vertical lines correspond to the phycocyanin absorption trough at about 620 nm, the chlorophyll-a absorption trough at about 675 nm, peak chlorophyll-a reflectance at about 700 nm, and NIR absorption by water at about 740 nm. The "red edge" region of the spectrum extends from 670 nm to 700 nm and indicates the presence of chlorophyll-a.

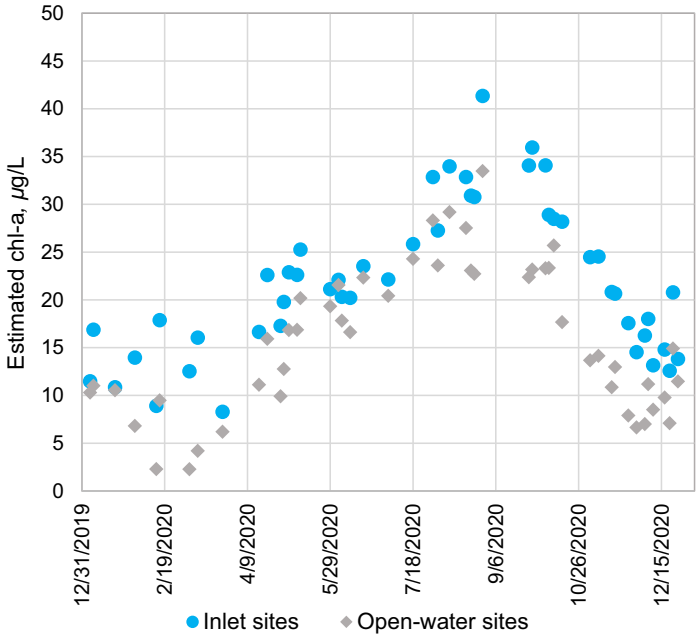

Fig. 10 Moses3b-Sen2Cor mean chlorophyll-a concentration estimation simulation reveals seasonal variation for the open-water and inlet sites, January 2020 to December of 2020.

was 19 μg/L at the inlet site and 18 μg/L at the open-water site, phycocyanin was 1.36 RFU at the inlet site and 1.16 RFU at the open-water site, and turbidity was 9.27 FNU at the inlet site and 3.26 FNU at the open-water site). The Secchi disk depth was observed to be greater at the open-water site (0.79 m), compared with the inlet site (0.39 m).

Finally, annual chlorophyll-a concentration was estimated across sampling sites from January to December of 2020. Chlorophyll-a concentrations were estimated from a 50 m diameter mean area for each open-water and inlet site from regional-scale cloud and sun-glint free satellite overpasses ($n = 49$). Seasonal variations in chlorophyll-a concentrations were observed for open-water and inlet sites (Fig. 10).

4 Discussion of Findings

The calibration and estimation of chlorophyll-a concentrations was implemented in a novel approach using the cloud-based platform for near real-time regional and time series monitoring of reservoirs in north Texas. The cloud-based platform facilitated efficient geoprocessing for sampling site selection and study design and visualization for analysis of the index-AC combinations over the study area. The historical Landsat archive was inspected using time-series tools to select reservoir sampling sites on the basis of interannual spectral reflectance to represent the range of spectral reflectance present across the study reservoirs. Estimates of chlorophyll-a concentrations were produced to reveal seasonal variation for open-water and inlet sites (Fig. 10). The seasonal patterns of estimated chlorophyll-a were consistent with seasonal patterns observed in the field data (Fig. 3) and with seasonal variation reported in the literature[12] (i.e., elevated aquatic chlorophyll-a during the warm season).

Data collected for the study[46] revealed that cyanobacteria primarily dominated during the warm season. Different spatial patterns in water-quality emerged between inlet and open-water sites. Consistent with Ref. 1, inlet sites exhibited more eutrophic aquatic conditions than open-water sites. Higher chlorophyll-a and turbidity values and shallower Secchi depths were observed at inlet sites compared with open-water sites (Table 2). Mean water temperatures were higher for the inlet sites (27.2°C) compared with the deeper open-water sites (25.4°C).

The Moses3b spectral index achieved the highest ranking across all index-AC combinations that were evaluated. The top performing index-AC combinations, as shown in Figs. 7 and 8, reveal relatively consistent patterns in the estimates of chlorophyll-a concentration, with concentrations generally higher in the inlet sites and lower in the open-water sites, e.g., consistent with

the patterns revealed at Grapevine Lake, August 19, 2020 (Fig. 9). Compared to open-water sites, the Moses3b-Sen2Cor combination delivered better linear agreement with chlorophyll-a field measurements at inlet sites where there was a greater abundance of near surface aquatic chlorophyll-a concentrations, and the overall chlorophyll-a reflectance signal was stronger (Fig. 9). An advantage offered by Sentinel-2 is the ability to detect chlorophyll-a at a higher spatial resolution on the range of tens of meters compared with coarser (300 m) spatial resolution available with the Sentinel-3 or with other water-quality monitoring methods that also rely on ocean color satellite sensors with a resolution that also is on the range of hundreds of meters. This finer resolution is particularly advantageous at inlet sites because it allows for detailed monitoring of these near shore areas that are frequented by people, pets, and wildlife.

The Moses three-band index utilizes Sentinel-2 spectral bands 4, 5, and 6 (Table 1). The algorithm was designed for aquatic chlorophyll-a detection in turbid coastal waters and was reported to have demonstrated potential for near real-time monitoring by Moses et al.[65] This index enables detection of chlorophyll-a for both cyanobacteria and other algae present on or entrained near the water surface in a turbid reservoir system. The response of bio-optical spectral features to water-quality provides further evidence of why the Moses3b approach performed well and is an example of why the authors of this study tested multiple spectral indices to optimize the performance for the study area. Indices BR54, NDCI54, and S23BDA were among the top ranked indices (Table 1) across all three ACs, and they captured the "red edge" portion of the spectrum (Fig. 9). The sensitivity of these wavelengths to aquatic chlorophyll-a is consistent with the literature.[25,26] This outcome is consistent with the findings reported in Ref. 27; when King et al. tested these same 17 algorithms, the red edge algorithms Moses3b and S23BDA delivered the highest accuracies. The Moses3b and S23BDA indices are similar (Table 1); both use the Sentinel-2 red (band 4), red edge (band 5), and an NIR band, but they use different parts of the NIR absorption spectra [Moses3b: band 6 (740 nm), S23BDA: band 8a (864 nm)] (Fig. 9), where there appears to be slightly less absorption of NIR in the 740 nm region of the electromagnetic spectrum compared with the 864 nm region, ultimately producing different chlorophyll-a estimation results. In addition, like the Moses3b algorithm, the normalized difference chlorophyll index (NDCI54) is reported to produce successful results for estimating chlorophyll-a in turbid productive waters.[65,66]

4.1 Limitations and Areas for Improvement in Real-Time Satellite Monitoring of Water-Quality

Challenges associated with detection of algae and cyanobacteria from satellite sensors are not unique to this study and are well documented.[25] Real-time earth observation requires robust approaches that are resilient to changes in dynamic environmental conditions including water-quality, phytoplankton communities, and atmospheric conditions. Satellite sensor technology is currently (2023) undergoing rapid development that is enabling advanced spectral resolution, increased overpass frequency, imaging across a range of spatial scales, interoperability and harmonization of satellite sensors, and high performance cloud platforms that facilitate advancements in geoprocessing and spatial data science.[27,36,72]

The chlorophyll-a concentration estimates described herein are limited to the *in-situ* matches between water-quality data and satellite imagery obtained during the study period. Because of the performance uncertainties described herein, chlorophyll-a concentrations estimated from satellite imagery would benefit from additional field observations for validation purposes. Deploying field crews across the region for *in-situ* water-quality monitoring coordinated with cloud-free satellite overpasses is logistically challenging. The detection and estimation process would benefit from the integration of additional data (e.g., from shore and buoy sensors[7]) to better inform and study the complexities of the dynamic reservoir systems observed across the north Texas region. Considering the relatively stronger performance at inlet sites, follow-up studies could benefit from calibration efforts that specifically target varying aquatic conditions observed within the reservoirs.

Chlorophyll-a estimations produced outliers for the highest chlorophyll-a observations in the *in-situ* dataset (chlorophyll-a: 87 μg/L; Secchi depth, 0.49 m at Lake Lavon, Site L1 on August 6, 2020) for the Moses3b approach across all ACs (Fig. 6). The Moses3b-ACOLITE combination yielded the second highest chlorophyll-a observation (chlorophyll-a: 83 μg/L; Secchi depth: 0.37 m at Lake Lavon, Site L1 on September 14, 2020). The Moses3b index combined with Sen2Cor and MAIN each generated a single negative estimate, when ACOLITE did not produce

negative estimated values. The minimum reporting limit for chlorophyll-a of 3 $\mu g/L$[49] is used for calibration and presents an opportunity for improvement in chlorophyll estimation <3 $\mu g/L$ because negative estimates are physically impossible. This study did not examine the intercomparison of the AC techniques and therefore cannot provide an explanation for why individual AC procedure performances achieve different outcomes; the use of AC factors is an ongoing topic of research in the remote sensing community.[30]

The cloud-based remote sensing platform facilitates the seamless integration of additional satellite sensors which would improve the likelihood of obtaining high-quality cloud and sun-glint-free image acquisitions. Sensors with expanded spectral resolution that can detect phycocyanin (e.g., Sentinel 3) could be ingested into the real-time earth observation system to leverage sensor assets and capabilities across multiple satellite platforms.[30] Cyanobacteria genera reveal unique hyperspectral signatures,[57] and when applied to space-borne hyperspectral imagery, they have demonstrated potential to differentiate aquatic cyanobacteria genera[72] advancing detection beyond chlorophyll-a and phycocyanin proxy estimators of algae and cyanobacteria.

Clouds, smoke, wind, and sun glint can impair the performance of satellite chlorophyll-a retrieval. Although AC routines and cloud cover masking are designed to correct for atmospheric effects on satellite detections, extensive cloud cover presents a physical limitation for real-time monitoring. Cloud cover is common in the study area. For example, in part of north Texas consistent with the study area, Wilson and Jetz[73] reported the presence of cloud cover in 47% of overpasses within the study area using high frequency daily MODIS satellite overpasses. As technology improves, cloud and cloud shadow detection and masking, as well as sun-glint correction techniques, will likely continue to advance the quality of near real-time earth imaging.

5 Conclusions

The U.S. Geological Survey, in collaboration with reservoir managers from the City of Dallas and North Texas Municipal Water District, developed a regional reservoir satellite monitoring system to aid in the ability to monitor algae and cyanobacteria across 10 water-supply reservoirs located primarily in north Texas. Water-quality sampling site visits were coordinated with Sentinel-2 satellite overpasses to match *in-situ* data with satellite imagery to estimate chlorophyll-a concentration, and to ascertain water-quality conditions. Seventeen chlorophyll-a retrieval indices were initially tested using the ACOLITE atmosphere correction and ranked by the coefficient of determination. The moderate to high performing indices were further tested and compared using the Sen2Cor and MAIN atmosphere corrections. The linear relation between *in-situ* Chlorophyll-a and satellite retrieval of chlorophyll-a were quantitatively evaluated for accuracy, precision, and bias across all sites, and differentiated by open-water sites, and inlet sites. The performance outcome was additionally compared to *in-situ* hyperspectral reflectance, phycocyanin, turbidity, Secchi depth, phytoplankton taxonomy, and other water-quality parameters. The Moses three-band spectral index designed for chlorophyll-a detection in turbid coastal waters delivered the highest ranked performance across all atmosphere correction procedures. Compared to open-water sites, the Moses3b-Sen2Cor combination delivered better linear agreement with chlorophyll-a field measurements at the near-shore inlet sites where there was a greater abundance of *in-situ* aquatic chlorophyll-a concentrations, and the overall chlorophyll-a hyperspectral reflectance signal was stronger. The chlorophyll-a concentration estimator was implemented in a cloud-computation remote sensing platform to reveal spatiotemporal patterns of aquatic chlorophyll-a from Sentinel-2 imagery. The methods applied herein provide expanded regional monitoring aiming to support water resource managers and interested members of the public in the identification of near real-time conditions across dynamic reservoir systems.

6 Appendix

Appendix Fig. 11(a)–(d) depicts the collection of Index-AC combinations correlated with *in-situ* chlorophyll-a ranked by the coefficient of determination (R^2). Appendix Fig. 12 presents the correlation of *in-situ* chlorophyll-a and *in-situ* turbidity which resulted in a low R^2 value. Appendix Fig. 13 presents the correlation between *in-situ* turbidity on the remotely sensed chlorophyll-a signal. R^2 values indicated that the influence of turbidity on the Moses3b index was consistently low.

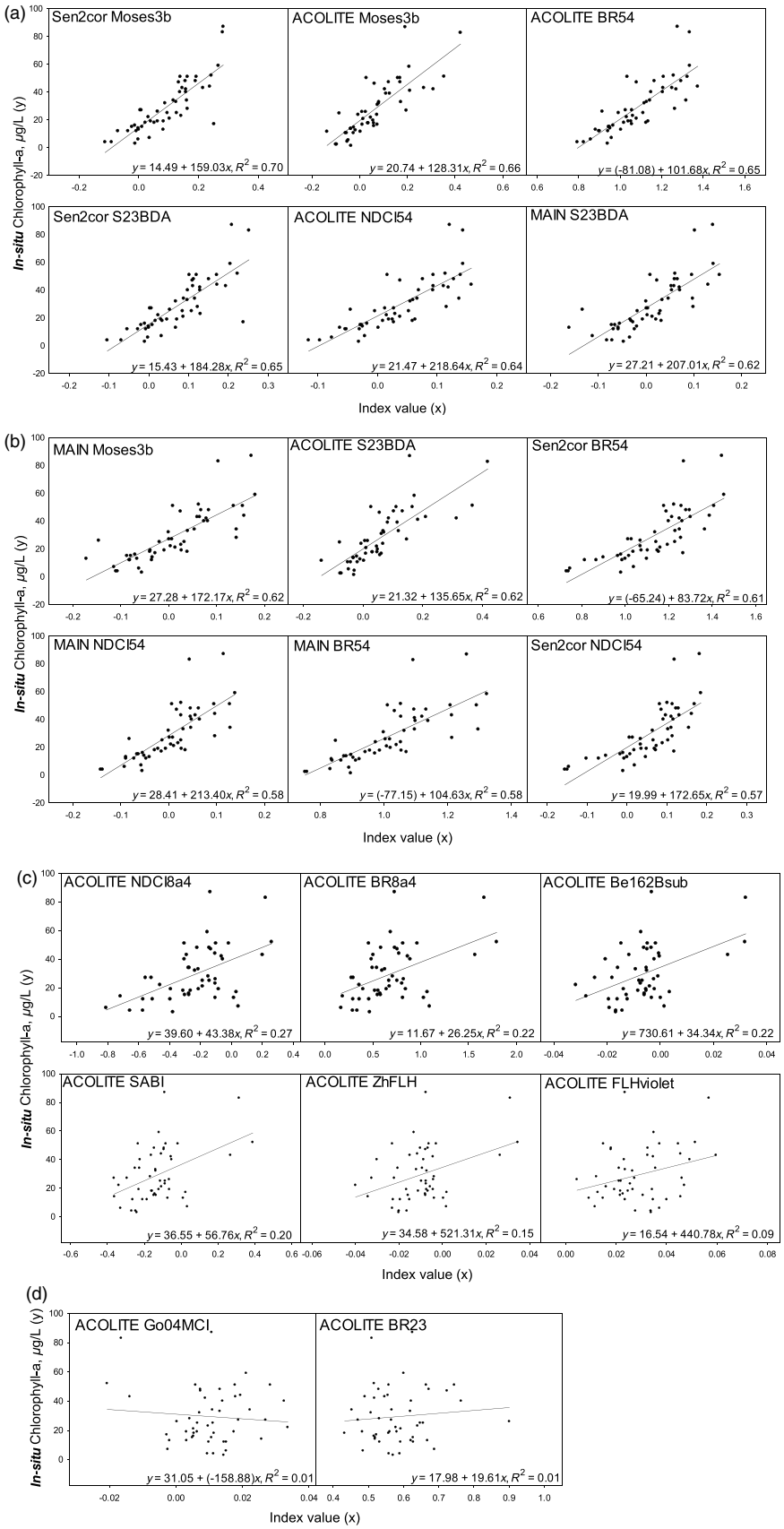

Fig. 11 (a)–(d) Index-AC combination scatterplots ranked by coefficient of determination (R^2) with linear regression equation.

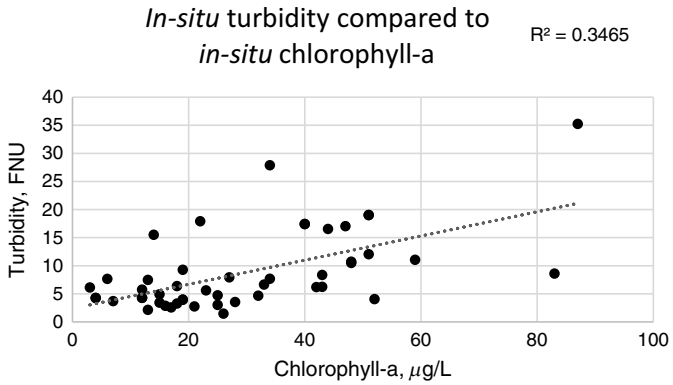

Fig. 12 *In-situ* turbidity, FNU, compared to *in-situ* chlorophyll-a μg/L ($N = 44$).

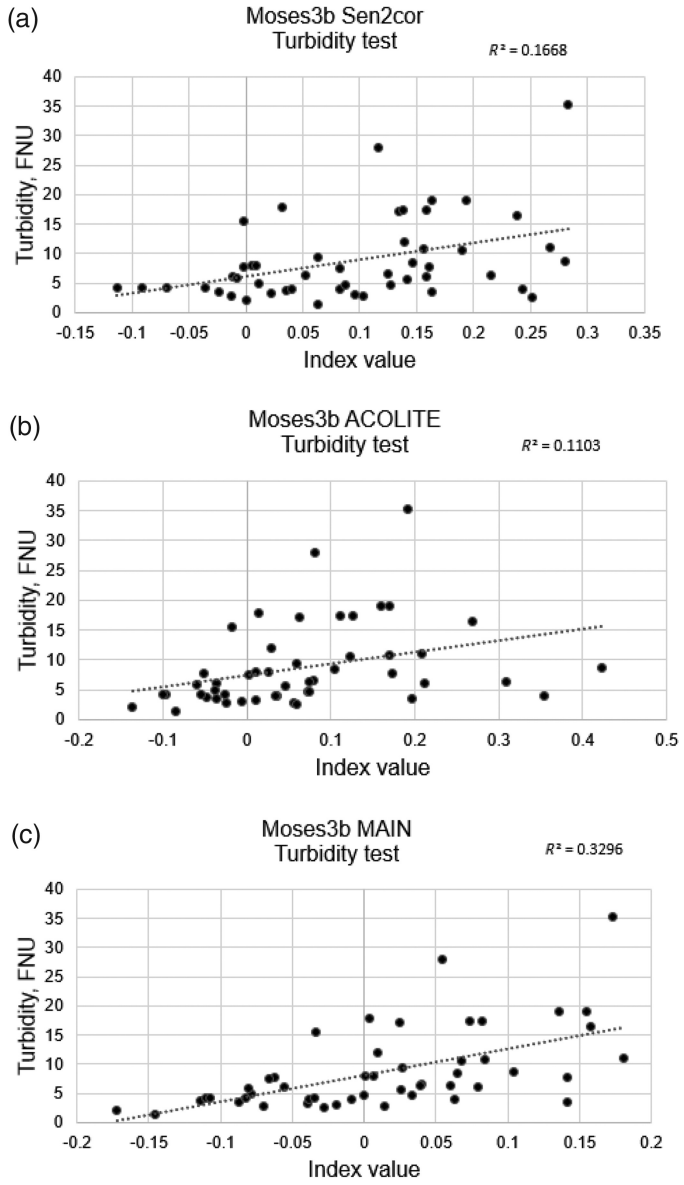

Fig. 13 *In-situ* turbidity compared to Moses3b for the Sen2Cor (a), ACOLITE (b), and MAIN (c) atmosphere corrections by coefficient of determination (R^2) ($N = 49$).

Table 4 ESA Sentinel-2a and Sentinel-2b MultiSpectral Instrument spectral band number, central wavelengths, bandwidth, and spatial resolution.[21]

	S2A		S2B		
Band number	Central wavelength (nm)	Bandwidth (nm)	Central wavelength (nm)	Bandwidth (nm)	Spatial resolution (m)
1	442.7	21	442.2	21	60
2	492.4	66	492.1	66	10
3	559.8	36	559	36	10
4	664.6	31	664.9	31	10
5	704.1	15	703.8	16	20
6	740.5	15	739.1	15	20
7	782.8	20	779.7	20	20
8	832.8	106	832.9	106	10
8a	864.7	21	864	22	20
9	945.1	20	943.2	21	60
10	1373.5	31	1376.9	30	60
11	1613.7	91	1610.4	94	20
12	2202.4	175	2185.7	185	20

Code and Data Availability

The data presented in the article are published as a U.S. Geological Survey data release available at https://doi.org/10.5066/P9X1R5IM. The data were processed with previously published algorithms as explained in the Methods section.

Author Contributions

- **Victoria G. Stengel:** Conceptualization, project development, investigation, methodology, remote sensing analysis, visualization, writing–original draft and Google Earth Engine developer.
- **Jessica M. Trevino:** Water-quality and biology analysis, project management, visualization, and writing–original draft.
- **Tyler V. King:** Methodology, remote sensing analysis, writing–original draft, and R and Google Earth Engine developer.
- **Scott Ducar:** Methodology, and writing–review and editing, and R developer.
- **Stephen Hundt:** Methodology, and writing–review and editing.
- **Konrad C. Hafen:** Methodology, and writing–review and editing.
- **Christopher J. Churchill:** Conceptualization, project development, project management, methodology, and writing–review and editing.

Acknowledgments

The authors thank Sean Wohltman, Yvan Aquino, Derrell Lee, Tyler Erikson, Toby Welborn, Willet Wilson, Samapriya Roy, August Scholtz, and Joe Vrabel for their contributions to the development of the near real-time monitoring system in the Google Earth Engine platform. Thank you to Nima Pahlevan for remote sensing of water quality science guidance during the conceptualization phase of this endeavor. We extend our gratitude to the known USGS peer reviewers Carl Legeiter and Michael Meyer and to the anonymous peer reviewers as well. Thank you to John Gordon for guidance, mentorship, and editing. Thank you to the USGS field crew who coordinated reservoir

water-quality sampling visits with satellite overpasses across the north Texas regional study area (during a global pandemic). Any use of trade, product, or firm names is for descriptive purposes only and does not imply endorsement by the U.S. Government.

References

1. I. Chorus and M. Welker, *Toxic Cyanobacteria in Water: A Guide to Their Public Health Consequences, Monitoring and Management*, 2nd ed., CRC Press, London (2021).
2. F. Jüttner and S. B. Watson, "Biochemical and ecological control of geosmin and 2-methylisoborneol in source waters," *Appl. Environ. Microbiol.* **73**(14), 4395–4406 (2007).
3. J. H. Landsberg et al., "A large-scale sustained fish kill in the St. Johns River, Florida: a complex consequence of cyanobacteria blooms," *Harmful Algae* **92**, 101771 (2020).
4. H. W. Paerl et al., "Harmful freshwater algal blooms, with an emphasis on cyanobacteria," *Sci. World J.* **1**, 76–113 (2001).
5. K. E. Havens, "Cyanobacteria blooms: effects on aquatic ecosystems," in *Cyanobacterial Harmful Algal Blooms: State of the Science and Research Needs*, H. K. Hudnell, Ed., Vol. **619**, pp. 733–747, Springer New York, New York (2008).
6. M. Mutoti, J. Gumbo, and A. Jideani, "Occurrence of cyanobacteria in water used for food production: a review," *Phys. Chem. Earth, Parts A/B/C* **125**, 103101 (2022).
7. R. Kiesling, R. Gary, and M. Gary, "Monitoring indicators of harmful cyanobacteria in Texas," U.S. Geological Survey Fact Sheet 2008–3009 (2008).
8. J. M. Trevino and C. B. Petersen, "Assessment of field and laboratory methods for the detection and analyses of cyanobacteria and cyanotoxins in Texas Reservoirs," U.S. Geological Survey Data Release (2020).
9. C. Churchill and S. Baldys, "USGS Zebra Mussel monitoring program for North Texas," U.S. Geological Survey Fact Sheet 2012–3077 (2012).
10. L. M. Dionisio Pires and E. Van Donk, "Comparing grazing by *Dreissena polymorpha* on phytoplankton in the presence of toxic and non-toxic cyanobacteria," *Freshwater Biol.* **47**(10), 1855–1865 (2002).
11. O. Sarnelle et al., "Complex interactions between the zebra mussel, *Dreissena polymorpha*, and the harmful phytoplankter, *Microcystis aeruginosa*," *Limnol. Oceanogr.* **50**(3), 896–904 (2005).
12. S. Stroming et al., "Quantifying the human health benefits of using satellite information to detect cyanobacterial harmful algal blooms and manage recreational advisories in U.S. Lakes," *GeoHealth* **4**(9), e2020GH000254 (2020).
13. N. Pahlevan, S. Ackleson, and B. Shaeffer, "Toward a satellite-based monitoring system for water quality," *EoS* **99**, 1–3 (2018).
14. M. M. Coffer et al., "Quantifying national and regional cyanobacterial occurrence in US lakes using satellite remote sensing," *Ecol. Indic.* **111**, 105976 (2020).
15. E. B. Murphy et al., "An explanation for the Florida east coast *Gymnodinium breve* red tide of November 1972," *Limnol. Oceanogr.* **20**(3), 481–486 (1975).
16. I. Robinson, "Satellite observations of ocean colour," *Philos. Trans. R. Soc. Lond. A* **309**(1508), 415–432 (1983).
17. J. M. Clark et al., "Satellite monitoring of cyanobacterial harmful algal bloom frequency in recreational waters and drinking water sources," *Ecol. Indic.* **80**, 84–95 (2017).
18. M. M. Coffer et al., "Satellite remote sensing to assess cyanobacterial bloom frequency across the United States at multiple spatial scales," *Ecol. Indic.* **128**, 107822 (2021).
19. B. N. Seegers et al., "Satellites for long-term monitoring of inland U.S. lakes: the MERIS time series and application for chlorophyll-a," *Remote Sens. Environ.* **266**, 112685 (2021).
20. B. A. Schaeffer et al., "Mobile device application for monitoring cyanobacteria harmful algal blooms using Sentinel-3 satellite ocean and land colour instruments," *Environ. Modell. Software* **109**, 93–103 (2018).
21. European Space Agency, "User guides - Sentinel-2 MSI - Sentinel Online - Sentinel Online," https://sentinels.copernicus.eu/web/sentinel/user-guides/sentinel-2-msi (accessed 2 March 2023).
22. K. Toming et al., "First experiences in mapping lake water quality parameters with Sentinel-2 MSI imagery," *Remote Sens.* **8**(8), 640 (2016).
23. N. Pahlevan et al., "Seamless retrievals of chlorophyll-a from Sentinel-2 (MSI) and Sentinel-3 (OLCI) in inland and coastal waters: a machine-learning approach," *Remote Sens. Environ.* **240**, 111604 (2020).
24. J. E. O'Reilly et al., "Ocean color chlorophyll algorithms for SeaWiFS," *J. Geophys. Res.* **103**(C11), 24937–24953 (1998).
25. R. P. Stumpf et al., "Challenges for mapping cyanotoxin patterns from remote sensing of cyanobacteria," *Harmful Algae* **54**, 160–173 (2016).
26. F. P. Maciel et al., "Challenges for chlorophyll-a remote sensing in a highly variable turbidity estuary, an implementation with sentinel-2," *Geocarto Int.* **38**(1), 2160017 (2023).

27. T. King et al., "Mapping the probability of freshwater algal blooms with various spectral indices and sources of training data," *J. Appl. Rem. Sens.* **16**(4), 044522 (2022).
28. D. R. Mishra et al., "Characterizing the vertical diffuse attenuation coefficient for downwelling irradiance in coastal waters: implications for water penetration by high resolution satellite data," *ISPRS J. Photogramm. Remote Sens.* **60**(1), 48–64 (2005).
29. T. T. Wynne et al., "Characterizing a cyanobacterial bloom in Western Lake Erie using satellite imagery and meteorological data," *Limnol. Oceanogr.* **55**(5), 2025–2036 (2010).
30. N. Pahlevan et al., "ACIX-Aqua: a global assessment of atmospheric correction methods for Landsat-8 and Sentinel-2 over lakes, rivers, and coastal waters," *Remote Sens. Environ.* **258**, 112366 (2021).
31. Q. Vanhellemont and K. Ruddick, "Atmospheric correction of metre-scale optical satellite data for inland and coastal water applications," *Remote Sens. Environ.* **216**, 586–597 (2018).
32. B. P. Page, L. G. Olmanson, and D. R. Mishra, "A harmonized image processing workflow using Sentinel-2/MSI and Landsat-8/OLI for mapping water clarity in optically variable lake systems," *Remote Sens. Environ.* **231**, 111284 (2019).
33. M. Main-Knorn et al., "Sen2Cor for Sentinel-2," *Proc. SPIE* **10427**, 1042704 (2017).
34. Q. Vanhellemont, "Adaptation of the dark spectrum fitting atmospheric correction for aquatic applications of the Landsat and Sentinel-2 archives," *Remote Sens. Environ.* **225**, 175–192 (2019).
35. N. Gorelick et al., "Google Earth Engine: planetary-scale geospatial analysis for everyone," *Remote Sens. Environ.* **202**, 18–27 (2017).
36. C. E. Woodcock et al., "Transitioning from change detection to monitoring with remote sensing: a paradigm shift," *Remote Sens. Environ.* **238**, 111558 (2020).
37. A. Velastegui-Montoya et al., "Google Earth Engine: a global analysis and future trends," *Remote Sens.* **15**(14), 3675 (2023).
38. Google, "Harmonized Sentinel-2 MSI: multispectral instrument, level-2A | Earth engine data catalog," Google Developers, https://developers.google.com/earth-engine/datasets/catalog/COPERNICUS_S2_SR_HARMONIZED (accessed 15 March 2023).
39. R. Kennedy et al., "Implementation of the LandTrendr algorithm on Google Earth Engine," *Remote Sens.* **10**(5), 691 (2018).
40. J. C. Ho, A. M. Michalak, and N. Pahlevan, "Widespread global increase in intense lake phytoplankton blooms since the 1980s," *Nature* **574**(7780), 667–670 (2019).
41. K. B. Tanner, A. C. Cardall, and G. P. Williams, "A spatial long-term trend analysis of estimated chlorophyll-a concentrations in Utah Lake using Earth observation data," *Remote Sens.* **14**(15), 3664 (2022).
42. C. Kislik et al., "Mapping algal bloom dynamics in small reservoirs using Sentinel-2 imagery in Google Earth Engine," *Ecol. Indic.* **140**, 109041 (2022).
43. M. F. C. Giannini et al., "Effects of low-salinity and high-turbidity waters on empirical ocean colour algorithms: an example for Southwestern Atlantic waters," *Contin. Shelf Res.* **59**, 84–96 (2013).
44. Texas Water Development Board, "View all Texas Lakes & reservoirs," https://www.twdb.texas.gov/surfacewater/rivers/reservoirs/ (accessed 2 March 2023).
45. T. S. Lowery, "Long-range water supply plan update – integrated pipeline project," 2018, https://dallascityhall.com/government/Council%20Meeting%20Documents/msis_2_long-range-water-supply-plan-update-integrated-pipeline-project_combined_022618.pdf (accessed 16 March 2023).
46. J. M. Sievers, V. G. Stengel, and J. M. Trevino, *Surface-Water Characteristics and Phytoplankton Taxonomy in Selected North Texas Reservoirs Using Biological, Hyperspectral, and Water-Quality Methods, 2019-2020*, U.S. Geological Survey (2022).
47. U.S. Geological Survey, "National field manual for the collection of water-quality data: U.S. Geological Survey Techniques of Water-Resources Investigations," variously dated, https://www.usgs.gov/mission-areas/water-resources/science/national-field-manual-collection-water-quality-data-nfm (accessed 17 September 2023).
48. R. B. Baird et al., Eds., *Standard Methods for the Examination of Water and Wastewater, Modified Method 10200H*, 23rd ed., American Public Health Association, American Water Works Association, and Water Environment Federation, Washington, DC (2017).
49. Texas Commission on Environmental Quality, "Quality assurance project plan Trinity river authority," Clean Rivers Program Water Quality Planning Division, Austin, TX, p. 76 (FY2020 to FY2021).
50. YSI, "YSI EXO2 multiparameter water quality Sonde," 2023, https://www.ysi.com/exo2 (accessed 3 March 2023).
51. Kestrel, "Kestrel 4500 weather & environmental meter in tactical dress with Bluetooth in olive drab," Kestrel Instruments, 2023, https://kestrelinstruments.com/kestrel-4500-weather-environmental-meter-in-tactical-dress-with-bluetooth-classic-in-olive-drab-1 (accessed 3 March 2023).
52. W. G. Crumpton, "A simple and reliable method for making permanent mounts of phytoplankton for light and fluorescence microscopy," *Limnol. Oceanogr.* **32**(5), 1154–1159 (1987).
53. A. M. Bergquist and S. R. Carpenter, "Limnetic herbivory: effects on phytoplankton populations and primary production," *Ecology* **67**(5), 1351–1360 (1986).

54. A. L. St. Amand, *Mechanisms Controlling Metalimnetic Communities and the Importance of Metalimnetic Phytoplankton to Whole Lake Primary Productivity*, University of Notre Dame (1990).
55. K. Olrik, "Methods for quantitative assessment of phytoplankton in freshwaters: P. 1: Sampling, processing, and application in freshwater environmental monitoring programmes," Rapport - Naturvaardsverket, Sweden (4860) (1998).
56. H. Hillebrand et al., "Biovolume calculation for pelagic and benthic microalgae," *J. Phycol.* **35**(2), 403–424 (1999).
57. T. Slonecker et al., "Hyperspectral reflectance characteristics of cyanobacteria," *Adv. Remote Sens.* **10**(03), 66–77 (2021).
58. Malvern Panalytical, "ASD HandHeld 2: Hand-held VNIR - Spectroradiometer | Product support | Malvern Panalytical," 2023, https://www.malvernpanalytical.com/en/support/product-support/asd-range/fieldspec-range/handheld-2-hand-held-vnir-spectroradiometer (accessed 3 March 2023).
59. European Space Agency, "User guides - Sentinel-3 OLCI - Sentinel Online - Sentinel Online," https://sentinels.copernicus.eu/web/sentinel/user-guides/sentinel-3-olci (accessed 2 March 2023).
60. R. Beck et al., "Comparison of satellite reflectance algorithms for estimating phycocyanin values and cyanobacterial total biovolume in a temperate reservoir using coincident hyperspectral aircraft imagery and dense coincident surface observations," *Remote Sens.* **9**(6), 538 (2017).
61. H. J. Gons, "A chlorophyll-retrieval algorithm for satellite imagery (Medium Resolution Imaging Spectrometer) of inland and coastal waters," *J. Plankton Res.* **24**(9), 947–951 (2002).
62. R. Beck et al., "Comparison of satellite reflectance algorithms for estimating chlorophyll-a in a temperate reservoir using coincident hyperspectral aircraft imagery and dense coincident surface observations," *Remote Sens. Environ.* **178**, 15–30 (2016).
63. E. J. Tebbs, J. J. Remedios, and D. M. Harper, "Remote sensing of chlorophyll-a as a measure of cyanobacterial biomass in Lake Bogoria, a hypertrophic, saline–alkaline, flamingo lake, using Landsat ETM+," *Remote Sens. Environ.* **135**, 92–106 (2013).
64. C. Le et al., "Evaluation of chlorophyll-a remote sensing algorithms for an optically complex estuary," *Remote Sens. Environ.* **129**, 75–89 (2013).
65. W. J. Moses et al., "Operational MERIS-based NIR-red algorithms for estimating chlorophyll-a concentrations in coastal waters: the Azov Sea case study," *Remote Sen. Environ.* **121**, 118–124 (2012).
66. S. Mishra and D. R. Mishra, "Normalized difference chlorophyll index: a novel model for remote estimation of chlorophyll-a concentration in turbid productive waters," *Remote Sens. Environ.* **117**, 394–406 (2012).
67. U. Bhangale et al., "Analysis of surface water resources using Sentinel-2 imagery," *Procedia Comput. Sci.* **171**, 2645–2654 (2020).
68. R Foundation, "R: The R project for statistical computing," 2023, https://www.r-project.org/ (accessed 2 March 2023).
69. B. N. Seegers et al., "Performance metrics for the assessment of satellite data products: an ocean color case study," *Opt. Express* **26**(6), 7404 (2018).
70. D. Helsel et al., "U.S. Geological Survey techniques and methods," in *Techniques and Methods*, Book 4, Chapter A3, 458 p. (2020).
71. U. S. Geological Survey, *USGS Water Data for the Nation*, U.S. Geological Survey (1994).
72. C. J. Legleiter et al., "Spectral mixture analysis for surveillance of harmful algal blooms (SMASH): a field-, laboratory-, and satellite-based approach to identifying cyanobacteria genera from remotely sensed data," *Remote Sens. Environ.* **279**, 113089 (2022).
73. A. M. Wilson and W. Jetz, "Remotely sensed high-resolution global cloud dynamics for predicting ecosystem and biodiversity distributions," *PLoS Biol.* **14**(3), e1002415 (2016).

Victoria G. Stengel is a geographer for the U.S. Geological Survey where she leads remote sensing science research and method development on interdisciplinary geoscience teams collaborating across USGS science centers, mission areas, university and interagency efforts. Her background includes investigations in water, energy, minerals, environmental health, landscape conservation, and climate change.

Tyler V. King is a research hydrologist with the U.S. Geological Survey. His work focuses on operationalizing academic research to produce techniques and datasets needed to support scientifically informed decision making.

Biographies of the other authors are not available.